

Disrupted asteroid P/2016 G1. II. Follow-up observations from the Hubble Space Telescope

F. Moreno

Instituto de Astrofísica de Andalucía, CSIC, Glorieta de la Astronomía s/n, 18008 Granada, Spain

fernando@iaa.es

J. Licandro

Instituto de Astrofísica de Canarias, c/Vía Láctea s/n, 38200 La Laguna, Tenerife, Spain, and

Departamento de Astrofísica, Universidad de La Laguna (ULL), E-38205 La Laguna, Tenerife, Spain

M. Mutchler

Space Telescope Science Institute, 3700 San Martin Drive, Baltimore, MD 21218, USA

A. Cabrera-Lavers

Instituto de Astrofísica de Canarias, c/Vía Láctea s/n, 38200 La Laguna, Tenerife, Spain, and

GRANTECAN, Cuesta de San José s/n, E-38712, Breña Baja, La Palma, Spain

N. Pinilla-Alonso

Florida Space Institute, University of Central Florida, Orlando, FL 32816, USA

and

F.J. Pozuelos

Instituto de Astrofísica de Andalucía, CSIC, Glorieta de la Astronomía s/n, 18008 Granada, Spain, and

and

Space Sciences, Technologies and Astrophysics Research (STAR) Institute, Université de Liège, allée du 6 Août 17, Liège, Belgique.

ABSTRACT

After the early observations of the disrupted asteroid P/2016 G1 with the 10.4m Gran Telescopio Canarias (GTC), and the modeling of the dust ejecta, we have performed a follow-up observational campaign of this object using the Hubble Space Telescope (HST) during two epochs (June 28 and July 11, 2016). The analysis of these HST images with the same model inputs obtained from the GTC images revealed a good consistency with the predicted evolution from the GTC images, so that the model is applicable to the whole observational period from late April to early July 2016. This result confirms that the resulting dust ejecta was caused by a relatively short-duration event with onset about 350 days before perihelion, and spanning about 30 days (HWHM). For a size distribution of particles with a geometric albedo of 0.15, having radii limits of 1 μm and 1 cm, and following a power-law with index -3.0 , the total dust mass ejected is $\sim 2 \times 10^7$ kg. As was the case with the GTC observations, no condensations in the images that could be attributed to a nucleus or fragments released after the disruption event were found. However, the higher limiting magnitude reachable with the HST images in comparison with those from GTC allowed us to impose a more stringent upper limit to the observed fragments of ~ 30 m.

Subject headings: Minor planets, asteroids: individual (P/2016 G1) — Methods: numerical

1. Introduction

Asteroid P/2016 G1 (Panstarrs) was discovered by R. Weryk and R. J. Wainscoat on CCD images acquired on 2016 April 1 UT with the 1.8-m Pan-STARRS1 telescope (Weryk & Wainscoat 2016). Its Tisserand parameter with respect to Jupiter (Kresák 1982) can be calculated as $T_J=3.38$, so that the object belongs dynamically to the main asteroid belt, yet showing cometary appearance. The first object of this type, and the best characterized so far, was discovered by E.W. Elst and G. Pizarro (Elst et al. 1996), currently designated as 133P/Elst-Pizarro. This object constitutes the target of a proposed European Space Agency Mission called Castalia (Snodgrass et al. 2017). This new class of objects in the Solar System today comprises about twenty members. The proposed activation mechanisms for these objects are very diverse, ranging from sublimation-driven to rotational instabilities. Jewitt et al. (2015) give an excellent review of the different objects discovered so far, their orbital stability, and their activation mechanisms.

In a previous paper (Paper I, Moreno et al. 2016), disrupted asteroid P/2016 G1 was observed with instrumentation attached to the GTC, from late April to early June, 2016,

and a Monte Carlo dust tail model of the ejecta was applied to obtain the dust physical properties. In this paper we report follow-up observations of P/2016 G1 acquired with the HST, during two epochs (late June and early July, 2016) and apply the same dust model to the images, to assess the validity of the model parameters over a longer temporal baseline.

2. Observations and data reduction

Observations of P/2016 G1 were performed using the Wide Field Camera 3 (WFC3) with the wide-band filter F350LP, which has an effective wavelength of 584.6 nm and a width of 475.8 nm. The object was observed on two epochs, June 28, and July 11, 2016. In the first observing run, 5 frames of 420 s exposure time each, were acquired. In the second, 4 images were taken, of 580 s exposure time each. Table 1 shows the log of the observations, where the observation times refer to the starting UT time at each observing date. Table 1 displays the relevant geometric parameters, namely the geocentric (Δ) and heliocentric (R) distances, the phase angle (α), the position angle of the extended Sun-to-asteroid radius vector ($PsAng$), and the angle between the Earth and target orbital plane ($PlAng$), this latter parameter showing values close to the latest GTC observation on June 8, 2016, so that the appearance of the object is similar to the GTC image of that date (see Paper I, figure 1, and compare with Fig. 1).

Our target was placed on the UVIS2 chip of WFC3, which provides an image scale of $0.04''/\text{px}$, giving pixel sizes of 46 km and 49 km at the asteroid on 28 June 2016 and 11 July 2016, respectively. At each epoch, our dithered images were median-combined, resulting in the rejection of background sources, cosmic rays, and bad pixels. As the object was so faint, the resulting combined images were binned $8\times$ in order to increase signal to noise ratio which becomes ~ 10 when averaged over the object. Since no nucleus or other spatial reference exists, the alignment procedure of the images was difficult, so that some blurring cannot be ruled out.

For the F350LP filter, we used a flux calibration factor (the so-called PHOTFLAM parameter) of 5.297×10^{-20} erg cm $^{-2}$ s $^{-1}$ Å $^{-1}$. The calibration formula, relating the $C = DN s^{-1}$ values of the image to surface brightness S is given by $S = (PHOTFLAM/\Omega)C$, where $\Omega=3.76\times 10^{-14}$ sr is the solid angle subtended by a pixel. The surface brightness values are finally converted to solar disk intensity units (i/i_0), which are the output units of the Monte Carlo dust tail code. To do this, we need to convolve the intensity of the mean solar disk spectrum (Cox 2000) with the filter response, which gives $i_0=2.23\times 10^6$ erg cm $^{-2}$ s $^{-1}$ Å $^{-1}$ sr $^{-1}$. We finally get $i/i_0 = 6.31 \times 10^{-13}S$.

The resulting combined images of the asteroid are shown in Fig. 1. It is apparent the lack of any condensation that could be attributed to a nucleus or a fragment that could result from a disruption event. The object presents a very diffuse structure, becoming much more diluted than in the images taken previously with the GTC (Paper I), although retaining the main features, the inverted C-shaped structure near the head with an inner darker region near the predicted nucleus position relative to the surrounding material, and a slight westward lobe, more clearly apparent in the June 28 image. The increasing diffuseness is clearly a consequence of the expected outward expansion of the disrupted material and the effect of radiation pressure. This will be tested in the modeling of the ejecta as described in the next section.

As a result of the disruption event, in Paper I we found no fragments larger than ~ 50 m (assuming a geometric albedo of $p_v=0.15$). In these observations the limiting magnitude (considering a signal-to-noise ratio $S/N=3$) of the HST combined images obtained with the F350LP in both observing dates would be $V \sim 27.2$ for a G2V star according to the HST exposure time calculator (<http://etc.stsci.edu/etc/input/wfc3uvis/imaging/>). We compute the absolute magnitudes as $H_v = V - 5 \log(R\Delta) - \beta\alpha$ where $\beta=0.03 \text{ mag deg}^{-1}$ is the adopted linear phase coefficient. For the geometric conditions of the observations (see Table 1), the absolute magnitudes become $H_v=23.7$ and $H_v=23.5$ on June 28 and July 11, respectively. Adopting the empirical equation $D = \frac{1329}{\sqrt{p_v}} 10^{-H_v/5}$ (Harris & Lagerros 2002), where D is the fragment diameter, those absolute magnitudes can be translated into fragment radii of 31 m and 34 m, respectively. Hence, no fragments larger than ~ 30 m in radius would remain from the asteroid disruption that produced the observed activity. However, since the limiting magnitude refers to a dark background and not to a source located within a faint coma, this is actually an optimistic size limit.

3. The Model

The Monte Carlo dust tail model is described in Paper I, and will not be repeated here. The input parameters of the model were the dust-loss rate as a function of time, and the particle velocities. A half-Gaussian function was adopted for the dust loss rate, which is defined by a peak activity \dot{M}_0 , located at the event onset t_0 , and having a half-width at half-maximum denoted by HWHM, which is a measure of the effective time span of the event. For the particle velocities, we adopted a random function of the form $v = v_1 + \zeta v_2$, where ζ is a random number in the $[0, 1]$ interval, and v_1 and v_2 were the fitting parameters. The remaining dust parameters were set to the following values: the particles were assumed to be distributed in a broad range of sizes from $r=1 \mu\text{m}$ to $r=1 \text{ cm}$, and following a power-law

differential size distribution with index $\kappa=-3$. The particles had a density of $\rho_p=1000$ kg m⁻³, and a geometric albedo of $p_v=0.15$. The phase function correction was performed using a linear phase coefficient of $\beta=0.03$ mag deg⁻¹, as given above, which is in the range of comet dust particles in the $1^\circ \leq \alpha \leq 30^\circ$ phase angle domain (Meech & Jewitt 1987). The particle ejection was assumed isotropic, except at the beginning of the event, where it was set to occur along a privileged direction for a short time interval. This ad-hoc assumption was made in order to explain the westward extension on the head, very clearly seen in the GTC images (see Paper I, figure 4), but very diffuse on these HST images. This direction was found to be given by $u_r \sim 0.98$, $u_\theta \sim 0.18$, $u_z \sim 0.08$, where (u_r, u_θ, u_z) are unit vectors defining a cometocentric reference system, with u_r pointing away from the Sun, u_θ is perpendicular to u_r in the orbital plane and opposite to the comet motion, and u_z is perpendicular to the orbital plane.

The application of those input model parameters to the HST images resulted in a good agreement, although the fits are still improved by increasing the peak dust loss rate from 7.6 kg s⁻¹ to 10.5 kg s⁻¹. Fig. 2 displays the measured and modeled contours, showing an excellent agreement. This demonstrates that the model parameters derived from the previous GTC images are compatible with the follow-up HST images, thereby providing stronger confidence on the validity of the results.

4. Conclusions

From the combined GTC and follow-up HST observations and the application of the dust tail modeling to the disrupted asteroid P/2016 G1, the following conclusions can be drawn:

1) Asteroid P/2016 G1 was activated 350_{-30}^{+10} days before perihelion, i.e., around 10th February 2016. The activity had a duration of 24_{-7}^{+10} days (HWHM). The total dust mass emitted was at least $\sim 2 \times 10^7$ kg, with a maximum level of activity of $\sim 8-11$ kg s⁻¹. The dust loss mass rate parameters were estimated assuming a power-law size distribution of particles between 1 μ m and 1 cm, with power index of $\kappa=-3.0$, geometric albedo of 0.15, and being emitted isotropically.

2) The isotropic ejection model is able to reproduce approximately the observed tail evolution of the disrupted target. An impulsive, short-duration ejection event in a privileged direction pointing approximately away from the Sun has been invoked to produce a dust feature near the head of the asteroid in the west direction. We hypothesize that this could be attributed to an impact that triggered the disruption of the asteroid.

3) The ejection velocities inferred from the dust model are very small, being in the range from 0.015 to 0.14 m s^{-1} , with an average value of $\sim 0.08 \text{ m s}^{-1}$, corresponding to the escape velocity of an object of 35 m radius and 3000 kg m^{-3} density. On the other hand, from the HST observations, we find that the upper limit to the fragment sizes in the image is $\sim 30 \text{ m}$. These results are consistent, and explain why we were not able to find any sizable fragment.

We are indebted to an anonymous reviewer for his/her useful comments that allowed us to improve our paper.

This paper is based on observations made with the NASA/ESA Hubble Space Telescope, obtained at the Space Telescope Science Institute, which is operated by the Association of Universities for Research in Astronomy, Inc., under NASA contract NAS 5-26555. These observations are associated with program #14524.

This work was supported by contracts AYA2015-67152-R and AYA2015-71975-REDT from the Spanish Ministerio de Economía y Competitividad (MINECO, Spain). J.L. gratefully acknowledges support from contract AYA2015-67772-R (MINECO, Spain). N.P.-A. acknowledges support for Program number HST-GO-14524 provided by NASA through a grant from the Space Telescope Science Institute, which is operated by the Association of Universities for Research in Astronomy, Incorporated, under NASA contract NAS5-26555. F.J.P. is supported by Marie Curie CO-FUND fellowship, co-founded by the University of Liège and the European Union.

REFERENCES

- Cox, A.N. 2000, *Allen's Astrophysical Quantities*, fourth edition. Springer-Verlag.
- Elst, E.W., Pizarro, O., Pollas, C., et al. 1996, *IAU Circ.*, No. 6456, #1.
- Harris, A.W., & Lagerros, J.S.V., 2002, *Asteroids III*, W. F. Bottke Jr., A. Cellino, P. Paolicchi, and R. P. Binzel (eds), University of Arizona Press, 205.
- Jewitt, D., Agarwal, J., Hsieh, H. 2015, *Asteroids IV*, P. Michel, F.E. DeMeo, and W.F. Bottke Jr. (eds), University of Arizona Press, 221.
- Kresák, L. 1982 *BAICz*, 33, 104
- Meech, K.J., & Jewitt, D.C., 1987, *A&A*, 187, 585
- Moreno, F., Licandro, J., Cabrera-Lavers, A., et al. 2016 *ApJ*, 826, L22

Snodgrass, C., Jones, G.H., Boehnhardt, H., et al. 2017, *Adv. Space Res.*, in press.

Weryk, R. & Wainscoat, R.J. 2016, *Central Bureau for Astronomical Telegrams*, 4269

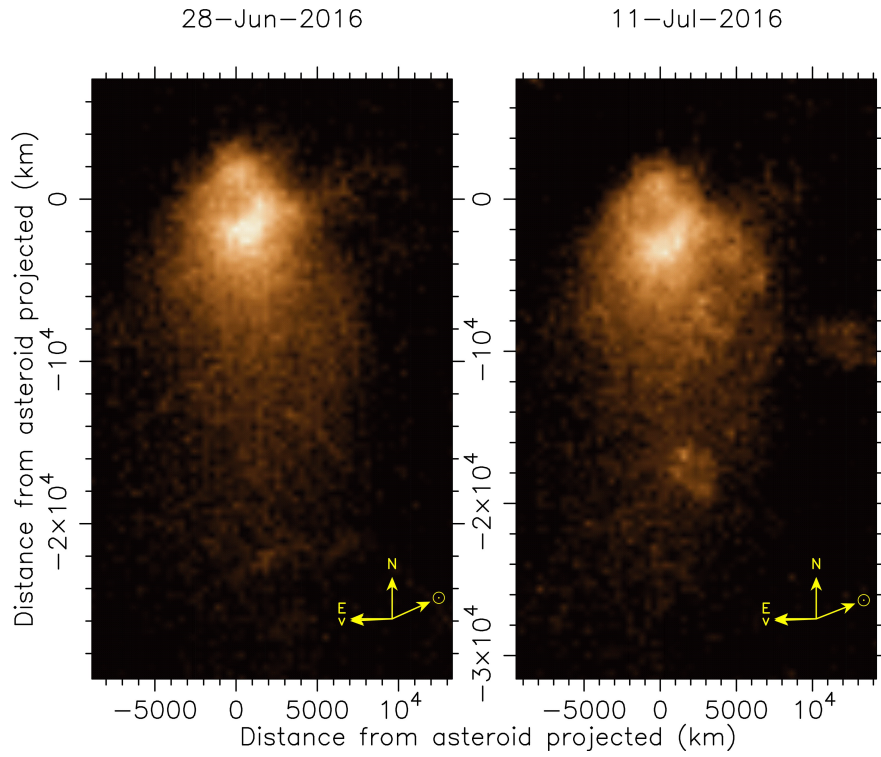


Fig. 1.— Drizzle-combined and $8\times$ binned images of P/2016 G1 obtained with WFC3 with the F350LP filter on the Hubble Space Telescope at the dates shown. The direction of the celestial North and East are indicated together with the Sun and the orbital velocity motion. Artifacts caused by imperfect removal of bright stars or galaxies are seen at coordinates $(2500, -18000)$ and $(12000, -9000)$ in the July 11 image.

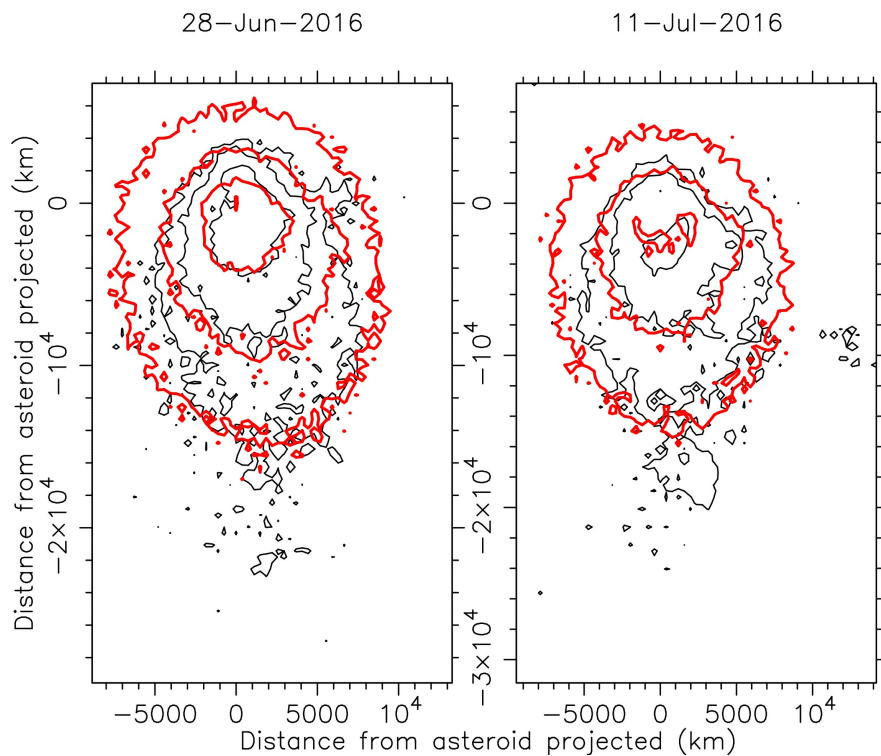


Fig. 2.— Measured (black contours) and modeled (thick red contours) isophotes for the two epochs as indicated. Innermost isophote levels correspond to 1.4×10^{-14} solar disk intensity units, and decrease in factors of two outwards. As in Fig. 1, North is up, and East to the left.

Table 1. Log of the observations

Start UT YYYY/MM/DD HH:MM	Days to perihelion	Total exp. time (s)	R (AU)	Δ (AU)	α ($^{\circ}$)	PtAng ($^{\circ}$)	PlAng ($^{\circ}$)
2016/06/28 14:53	-211.6	2100	2.318	1.592	21.3	114.28	-6.67
2016/07/11 10:42	-198.8	2320	2.290	1.698	24.2	114.45	-6.52